Aerodynamic Performance Analysis of E387 and S1010 Turbine Blade Profile

Dinh Quy Vu [1], Van Y Nguyen[1], Thi Tuyet Nhung Le[1,*]

[1]Hanoi University of Science and Technology, Hanoi, Vietnam

Abstract

INTRODUCTION: The two selected airfoils, EPU-E387 and EPU-S1010, are newly developed and have not yet been studied for their aerodynamic performance.
OBJECTIVES: This paper investigates the changes in lift and drag coefficients, as well as the lift-to-drag ratio, of two airfoils designed for small wind turbines operating at low Reynolds numbers. The results include 2D simulations performed using the commercial software ANSYS Fluent 2019.
METHODS: The research method involves varying the angle of attack to determine the optimal angle and identify which airfoil offers greater stability. The Reynolds numbers applied in the 2D simulations include 50,000, 60,000, 90,000, and 120,000.
RESULTS: The simulation results indicate that the EPU-E387 airfoil achieves the highest lift-to-drag coefficient at the optimal angle of attack, which is 13.13% greater than that of the EPU-S1010 airfoil at Reynolds number 120,000.
CONCLUSION: The EPU-E387 airfoil demonstrates greater stability compared to the EPU-S1010 at higher angles of attack.

1. Introduction

In 2022, the renewable energy sector experienced record-breaking growth, especially in wind power, which saw a 14% increase in output [1]. Solar and wind energy accounted for 90% of the renewable power additions, contributing significantly to the goal of achieving net zero emissions by 2050 [2]. However, some studies suggest that solar energy can release harmful substances like lead and cadmium, which pose risks to both human health and the environment [3]. This highlights the need for careful research and implementation in the use of solar energy. In contrast, wind energy continues to demonstrate strong potential for growth and is considered environmentally sustainable.

A wind turbine is a device that converts the kinetic energy of wind into electricity for practical use. The blades of the turbine are crucial for this process, requiring aerodynamic shape and advanced manufacturing techniques. The aerodynamic quality of the airfoil is a key factor in determining the performance of energy extraction. Research on airfoil optimization is the focus of many scientific studies. Arslan Saleem and Man-Hoe Kim [4] used genetic algorithms to optimize the NACA 9415 airfoil. Their results demonstrated a 1.25-fold increase in capacity and a "power augmentation ratio of 2.1 compared to the Betz limit." Genetic algorithms are widely applied in airfoil optimization. One study [5] combined this method with the HARP Opt code to optimize an antifouling airfoil, USP07-45XX, calculating an energy output of 4.787×10^4 kWh. Xu Zhang et al. [6] extended optimization to airfoils under freezing conditions, where the optimized NACA0012BT exhibited stable aerodynamic performance across angles of attack during freezing. Since turbines operate in varied conditions, another study [7] optimized airfoils for low wind velocities. The new airfoils developed in this research showed improved stability and efficiency in real-world applications.

Optimization in 3D modeling has also been extensively studied. Along with the length of wind turbine blades,

---

* Corresponding author. E-mail: nhung.lethituyet@hust.edu.vn

parameters such as airfoil shape, twist angle, and sweep angle can vary. Abdelaty et al. [8] investigated the torque differences between twisted and untwisted blades using Blade Element Momentum (BEM) theory with the NACA 4418 airfoil. Their findings showed that untwisted blades increased torque by 8-10% compared to twisted blades. Ahmed Mohamed et al. [9] conducted experimental tests to validate these results, also testing with the NACA 0012 airfoil. The experiments yielded similar differences between the two blade types, and the results indicated that the discrepancies between theoretical predictions and experimental findings were minimal.

A study of Mohammed G.K et al. [10] investigated the effects of dust on the performance of wind turbines. Over time, dust accumulation increases the roughness of the blades due to corrosion and adherence to the surface. The results indicated that dust leads to reduced lift and increased drag, ultimately diminishing energy output. Additionally, the impact of roughness varies depending on the Reynolds number and the specific type of airfoil used. Along with dust, rain can also cause erosion of wind turbine blades. Hoksbergen et al. [11] conducted a comprehensive study on leading-edge erosion caused by rain, focusing on the properties of droplet materials. This research developed a pressure model applicable to solid surfaces, enabling calculations for the lifespan of the blades based on fatigue analysis. In contrast to the effects of rain and dust, ice accumulation causes airfoils to thicken and alter their shape. A study of Linyue G. et al. [12] on short-duration ice accretion lasting 600 seconds revealed significant changes in lift and drag, with lift decreasing by 12% and drag increasing by 4.5 times compared to the original performance.

All the research topics mentioned above include an essential calculation step concerning the aerodynamic efficiency of wind turbine airfoils. The study by Abdulkareem et al. [13] examined three airfoils—NREL S830, SG6043, and SD7062—by varying the angle of attack and thickness using numerical simulations with ANSYS FLUENT. The findings were compared to reference data,

showing favorable results. Given that the length of the blade is substantial in relation to its chord, various sections from the base to the tip of the blade encounter different wind velocities and Reynolds numbers. As a result, a separate study of Haseeb S. et al. [14] explored the impact of Reynolds numbers on the aerodynamic performance of the airfoil, revealing that variations in the Reynolds number also affect the optimal angle of attack for that airfoil. Nhung L.T.T et al. [15] also identified factors that affect the aerodynamic quality of the S830 wing under conditions of velocity, Reynolds and environmental conditions such as ice buildup. In this study, the same approach as the study of Nhung L.T.T et al. [15] applied to two smaller thickness profiles, E387 and S1010. This research will leverage the commercial software ANSYS FLUENT to calculate, assess, and simulate the aerodynamic performance of two wind turbine airfoils: EPU-S1010 and EPU-E387. The findings will help identify the superior airfoil, and the subsequent phase of the project will involve experiments conducted in the AF6116 wind tunnel.

2. Numerical and method analysis

With the goal of manufacturing wind turbines to be installed in northern mountainous regions of Vietnam such as Sapa, wind turbines with capacities ranging from 100-400W are the research focus. Based on a survey of several types of turbine blades available in the market (Table1), some commonly used airfoils for these wind turbines are: NACA 0018, S1210, S1046, S830.

In the study by Le et al. [15], the airfoil thickness has a significant impact on aerodynamic quality. The authors also indicated that the aerodynamic efficiency of the profile increases when the thickness decreases to 20%. The E387 and S1010 profiles have relatively thinner profiles compared to the S830. These two profiles will be the subjects of this study, in order to compare the aerodynamic performance of the S830 blade with the same chord length.

Table 1. Survey of the small-scale wind turbine's parameters

N◦	Airfoil	N◦ of blades	Diameter (D-m)	Span (L-m)	Chord (c-m)	Ratio L/c	Power (W)	Wind speed (m/s)
1	SG6043	3	0.56	0.28	0.383	0.73	10	5
2	S826	3	0.944	0.421	0.072	5.85	40	6
3	S600	6	1.3	0.58	0.09	6.44	60	1.3-8
4	S400	3	1.2	0.58	0.08	7.25	60	2-13
5	S800	6	1.2	0.58	0.08	7.25	80	1.3-8
6	NACA4415	3	1.5	0.75	0.1	7.50	80	8
7	S600	5	1.1	0.53	0.07	7.57	60	2-10
8	NACA0018	3	1.75	0.81	0.1	8.10	150	2-13
9	S1210	3	1.75	0.8	0.09	8.89	400	2.5-11
10	S1046	3	1.28	0.6	0.067	8.96	360	2-8
11	S413	3	1.27	0.635	0.065	9.77	100	6

| 12 | S830 | 3 | 0.8 | 0.4 | 0.09 | 4.44 | 100 | 8 |
| 13 | S830 | 3 | 56 | 28 | 4.2 | 6.67 | 1000 | 8 |

2.1. Numerical analysis

The two airfoils selected are the recently developed EPU-S1010 and EPU-E387. These are two airfoils developed from the original airfoils S1010 and E387 respectively with changes in maximum thickness, maximum position, maximum camber, and maximum camber position values to achieve better aerodynamic efficiency. The shape of the two wings can be shown in the ICEM CFD in Fig. 1 and Fig. 2.

Figure 1. Airfoil EPU-E387

Figure 2. Airfoil EPU-S1010

In all flow scenarios, ANSYS FLUENT addresses the conservation equations for mass and momentum. For various flow types, such as heat transfer, compressibility, and mixing, additional methods are incorporated [16]. The continuity equation, which represents the conservation of mass, can be expressed as follows:

$$\frac{\partial \rho}{\partial t} + \nabla . (\rho \vec{v}) = S_m \qquad (1)$$

Equation (1) is the general expression for the mass conservation equation and is valid for both incompressible and compressible flow scenarios.

Momentum conservation in an inertial (non-accelerating) reference frame is expressed as:

$$\frac{\partial}{\partial t}(\rho \vec{v}) + \nabla . (\rho \vec{v} . \vec{v}) = -\nabla p + \nabla . (\overline{\overline{t}}) + \rho . \vec{g} + \vec{F} \qquad (2)$$

The calculated values for the outputs of the C_L and C_D values are calculated by ANSYS Fluent based on the following equations:

$$C_L = \frac{L}{\frac{1}{2}\rho U^2 C\, l} \qquad (3)$$

$$C_D = \frac{D}{\frac{1}{2}\rho U^2\, l} \qquad (4)$$

Wind turbines typically operate under natural conditions at relatively low wind speeds, ranging from 5 to 20 m/s. Therefore, the Spalart-Allmaras turbulence model is selected for calculations. This model offers the advantage of rapid computation, as it uses only one parameter, and is well-suited for low-velocity flows. In the Spalart-Allmaras model, fluctuations resemble turbulent kinematic viscosity, except in the vicinity of the boundary layer, where viscosity has an effect. The dynamic equation for the variable chaotic viscosity is:

$$\frac{\partial}{\partial t}(\rho \tilde{v}) + \frac{\partial}{\partial x_i}(\rho \tilde{v} u_i) = G_v + \frac{1}{\sigma_{\tilde{v}}}\left[\frac{\partial}{\partial x_j}\left\{(\mu + \rho \tilde{v})\frac{\partial \tilde{v}}{\partial x_j}\right\} + C_{b2}\rho\left(\frac{\partial \tilde{v}}{\partial x_j}\right)^2\right] - Y_v + S_{\tilde{v}} \qquad (5)$$

2.2. 2D simulation and meshing

In this study, ICEM CFD is utilized to define and create the computational grid model based on the input airfoil. To ensure that the calculation results are not affected, the computational model's boundary must be large enough. A C-shaped boundary is selected for the calculation area, as it is well-suited for 2D meshing of the airfoil. The leading edge of the airfoil closely resembles the shape of the letter C, which enhances the meshing process. The airfoil has a chord length of C = 0.3 m. The C-domain is developed using ICEM CFD, and its dimensions consist of a C-radius of 10C and a rear area measuring 30C. Fig. 3 provides detailed measurements.

To guarantee the accuracy of the calculations, four different grid sizes were created to evaluate grid convergence. Each mesh features an increasing number of elements while maintaining the same minimum element size near the airfoil boundary. The four grid sizes consist of 28,689, 60,984, 81,679, and 128,384 elements, respectively. All grid models ensure a y+ value of less than 1, with a growth rate value of 1.2. Grid models 1 through 4 gradually reduce the element length size on the airfoil surface, while maintaining the same height size. This paper will compare the values calculated from ANSYS Fluent across these four grids to assess the differences between them. The results are summarized in Table 2.

Table 2. Difference of grids

No. of elements	C_L	Difference of C_L	C_D	Difference of C_D
28.689 (GRID 1)	0.8840	N/A	0.6324	N/A
60.984 (GRID 2)	0.8853	0.148%	0.6299	0.407%
81.679 (GRID 3)	0.8868	0.162%	0.6294	0.071%
128.384 (GRID 4)	0.8873	0.062%	0.6293	0.021%

In conclusion, the grid shows good convergence, with grid 3 being the optimal choice. It has deviations of only about 0.062% for the lift coefficient (CL) and 0.021% for the drag

coefficient (CD) when compared to grid 4. Since grid 3 has only two-thirds the number of elements of grid 4, it is considered the more efficient option (refer to grid 3 in Fig. 4).
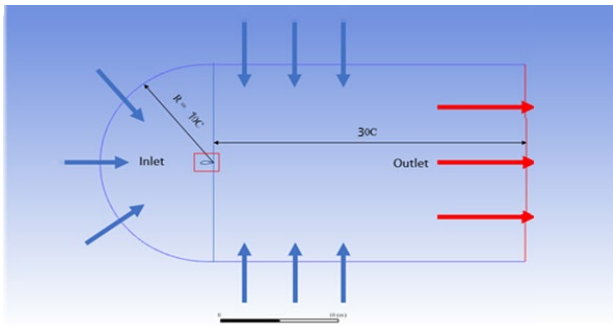

Figure 3. Fluid domain dimension

2.3. Method and boundary set-up

Table 3 presents the general parameters and research settings for the 2D model. The velocity defined at the velocity inlet in the table is based on the Reynolds number under investigation. In this study, COUPLE pressure–velocity coupling was used. The coupled scheme achieves a robust and efficient implementation for single-phase steady-state flows, offering superior performance when compared to segregated solution schemes [16].

Table 3. Method and boundary set-up

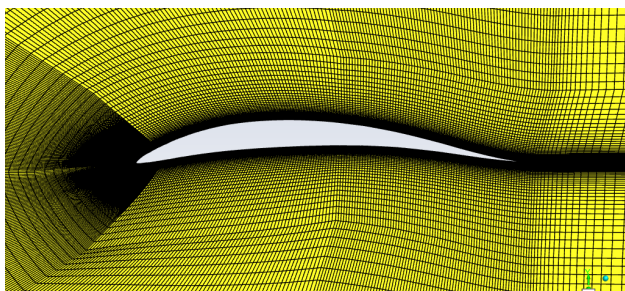| Mesh	C-grid, No. of element: 81.679
Turbulence	Spalart-Allmaras model
Fluid	Air, density 1.225 kg/m3 and viscosity 1.7894e-05 Kg/ (m.s)
Method	Second order accuracy. COUPLE pressure–velocity coupling was used
Convergence criteria	Less than 10e-5
Boundary conditions	Inlet: Velocity inlet, Outlet: Pressure outlet
	Turbulence intensity: 5%
	Airfoil: Wall, no slip

Figure 4. Grid 3 on airfoil VAST-EPU-E387

3. Result and discussion

3.1. Identification of the Optimal AoA

The angle of attack is a crucial factor influencing the aerodynamic performance of the airfoil. At the optimal angle of attack (AoA), the lift-to-drag ratio (CL/CD) can be significantly improved compared to non-optimal cases. This occurs because varying the angle of attack alters the pressure difference between the top and bottom surfaces of the airfoil, thereby affecting the CL/CD ratio. The simulation results illustrate the relationship between the CL/CD coefficient and the angle of attack for the two airfoils, EPU-S1010 and EPU-E387. The results are presented in Fig. 5, which depicts the CL/CD plot as a function of the angle of attack at a Reynolds number of 120,000 for both airfoils. The results indicate that the lift-to-drag coefficient (CL/CD) gradually increases with the rising angle of attack. However, once the angle of attack surpasses the optimal level, the CL/CD coefficient begins to decrease. For the airfoil EPU-E387, the optimal angle of attack is identified at 5 degrees, where CL/CD = 48.730, with the stall angle occurring at 10 degrees (Figure 5a). In contrast, the optimal angle of attack for the airfoil EPU-S1010 is found to be 4 degrees, yielding a CL/CD of 43.073, while its stall angle is at 9 degrees (Figure 5b).
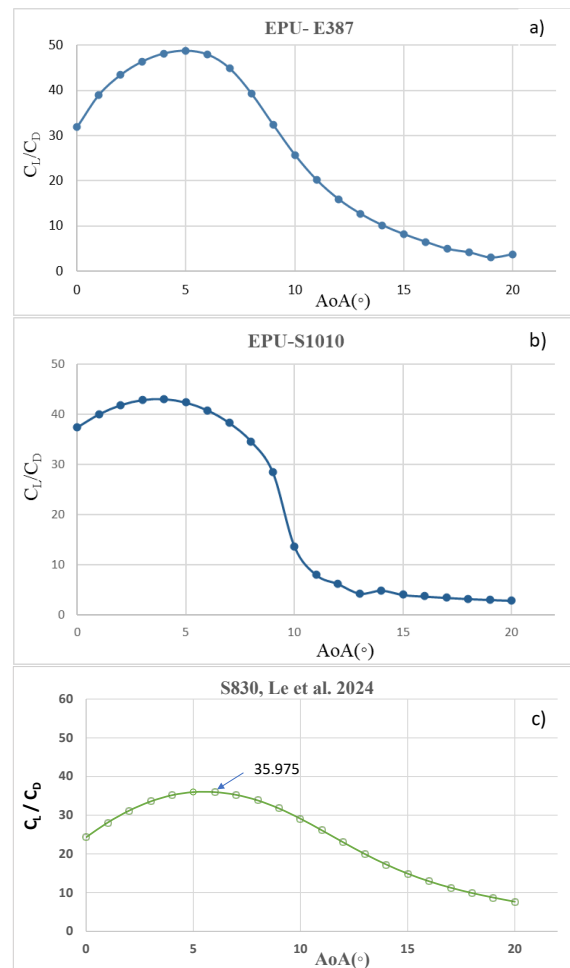

Figure 5. C_L/C_D vs AoA of airfoils at Reynolds number

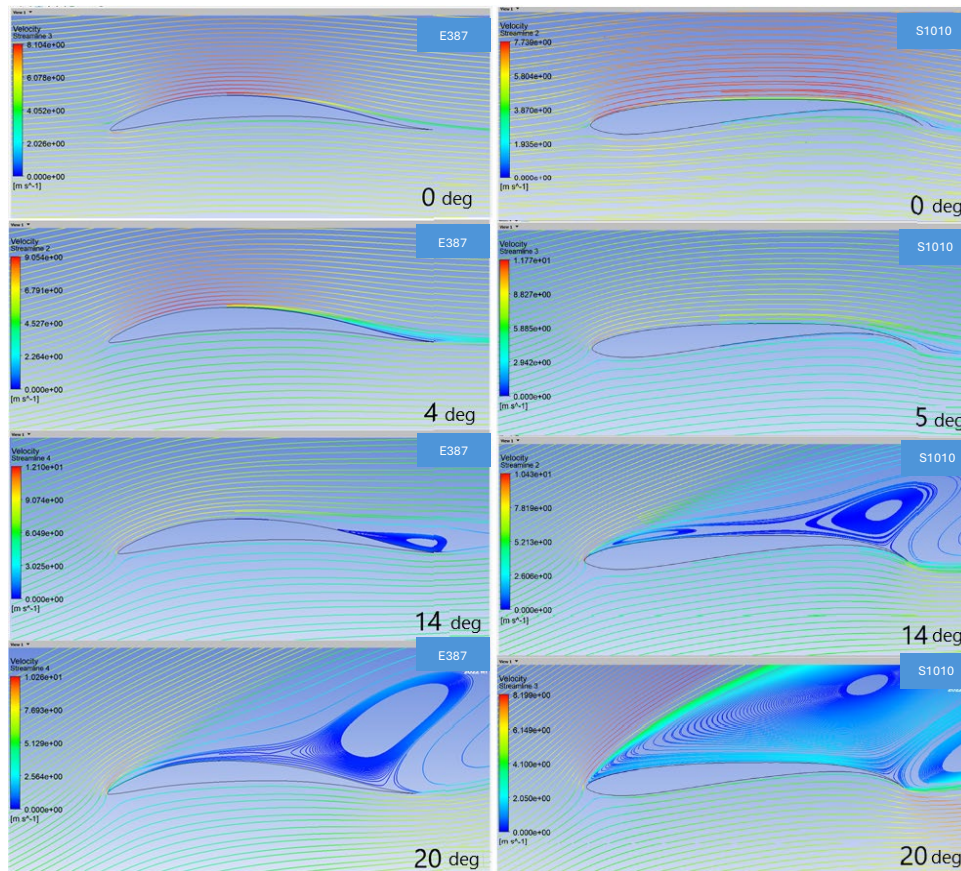120.000: a) EPU-E387; b) EPU-S1010; c) S830 (Le et al.2024).

Figure 1. Velocity distribution and flow separation in two airfoils E387 and S1010

Relative to the peak aerodynamic efficiency coefficient of the S830 at a Reynolds number of 120,000 (Fig. 5c), the E387 profile achieves a 26.16 % higher aerodynamic coefficient, while the S1010 profile exhibits a 16.47 % improvement. This highlights the E387 profile's superior aerodynamic performance over the other two profiles.

Along with having a higher CL/CD at its optimal angle of attack, the airfoil EPU-E387 also displays a lower slope in the CL/CD graph and a lower stall angle compared to the EPU-S1010. This deceleration is caused by flow separation. Fig. 6 illustrates this effect through velocity distribution plots on the airfoil. The angles of attack shown include the optimal angle and three additional angles: 0, 14, and 20 degrees.

The velocity distribution results shown in Fig. 6 also illustrate the stability of the EPU-E387 airfoil at elevated angles of attack. This stability is reflected in the level of flow separation experienced by the two airfoils. In general, the EPU-E387 airfoil exhibits less severe flow separation at the same angle of attack compared to the EPU-S1010. For instance, at an angle of attack of 14 degrees, flow separation on the EPU-E387 airfoil occurs about two-thirds along the chord length, while the EPU-S1010 experiences flow separation near the leading edge.

3.2. Influence of Reynold number in aerodynamic performance

This study broadens the range of Reynolds numbers to include 50,000, 60,000, and 90,000. The CL/CD values at the optimal angle of attack for both the EPU-E387 and EPU-S1010 airfoils are displayed in Tables 3 and Tables 4. The outcomes of the Reynolds number (Re) expansion for the two airfoils are depicted in Fig. 7 and Fig. 8.

Table 4. Optimal angle of attack and CL/CD airfoil EPU-E387

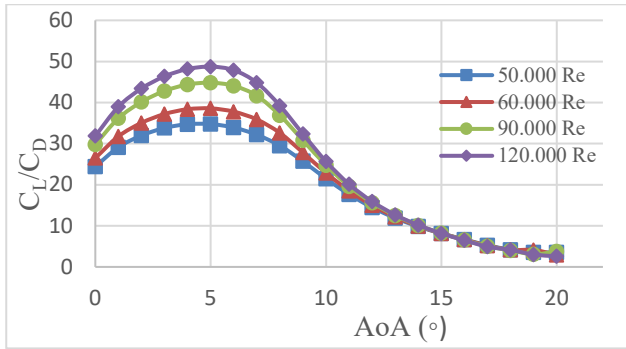| Re	50.000	60.000	90.000	120.000
Optimal AoA	5	5	5	5
CL/CD	34.7610	38.5775	44.8305	48.7304

Figure 7. CL/CD vs AoA and Re airfoil EPU-E387

At Reynolds numbers of 50,000, 60,000, 90,000, and 120,000, the optimal angle of attack for the EPU-E387 airfoil is consistently found to be 5 degrees. The study indicates that the CL/CD ratio increases as the Reynolds number rises within this range, which is consistent with the findings of the reference study [14]. Although CL/CD generally improves with increasing Reynolds number, at angles of attack exceeding 13 degrees, the CL/CD values across all four cases are almost identical.
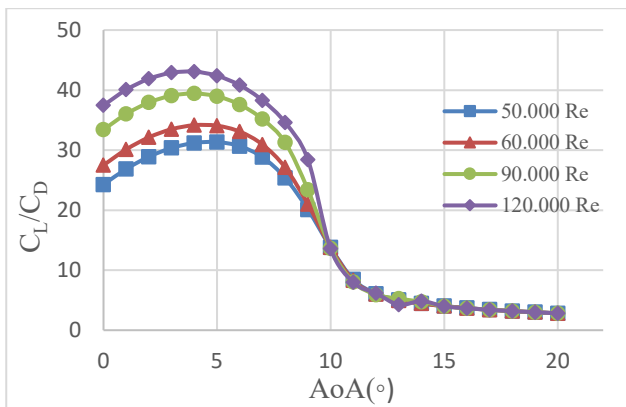

Figure 8. CL/CD vs AoA and Re airfoil EPU-S1010

Table 5. Optimal angle of attack and CL/CD airfoil EPU-S1010

Re	50.000	60.000	90.000	120.000
Optimal AoA	5	4	4	4
CL/CD	31.3438	34.1524	39.4378	43.0739

The EPU-E387 airfoil, which has a CL/CD value that is 13% higher at the optimal angle of attack at Reynolds 120,000 and shows greater stability with flow separation, is superior to the EPU-S1010 for practical use. The experimental phase will utilize the EPU-S1010 airfoil to compare it with the results from the 2D simulations.

The comparison results on aerodynamic performance between the two airfoils EPU-E387 and EPU-S1010 in this study and the S830 airfoil in the study by Nhung L.T.T et al. [15] within the same Reynolds number range show that the S830 airfoil has a lower CL/CD ratio compared to both other airfoils. Specifically, at the optimal angle of attack and a Reynolds number of 100,000, the S830 airfoil has a CL/CD ratio that is 26.16% lower than the EPU-E387 airfoil and 16.47% lower than the EPU-S1010 airfoil. Following the results of the numerical analysis, the EPU-E387 wing model was selected for fabrication as a physical model using 3D printing. In the next phase, it will undergo experimental testing in a wind tunnel to measure lift and drag coefficients.

4. Conclusion

This study analyzed the aerodynamic performance of two wind turbine airfoils, EPU-E387 and EPU-S1010, focusing on the optimal lift-to-drag ratio and angle of attack using the commercial software ANSYS FLUENT. The investigation, which explored Reynolds' numbers of 50,000, 60,000, 90,000, and 120,000, showed that the changes in the lift-to-drag coefficient were consistent with findings from earlier studies on other airfoils. At a Reynolds number of 120,000, the results indicate that the EPU-E387 airfoil achieves a lift-to-drag ratio that is 13.13% greater than that of the EPU-S1010 at its optimal angle of attack. Furthermore, the velocity distribution results reveal that the EPU-E387 airfoil maintains better stability at higher angles of attack, as demonstrated by flow separation patterns. Therefore, the EPU-E387 airfoil is considered more suitable for application in wind turbines at low flow velocities. Future work will involve experimental testing of a wing model designed with 3D printing technology based on the EPU-E387 airfoil.

Nomenclature

AoA	Angle of attack
C_L	Lift coefficient
C_D	Drag coefficient
C_L	Lift coefficient
C_L/C_D	lift-to-drag ratio
ρ	Fluid density
p	Pressure
t	time
v	velocity vector field of the fluid
F	External body forces
S_m	Mass added to the continuous phase

References

[1] "Wind - IEA," ww.iea.org, 2022.

[2] "RENEWABLES 2022 GLOBAL STATUS REPORT," www.ren21.net, 2022.

[3] "End-of-Life Solar Panels: Regulations and Management," www.epa.gov, 2022.

[4] Arslan S., Man-Hoe K., "Aerodynamic performance optimization of an airfoil-based airborne," Energy, vol. 203, pp. 117841, 2020.

[5] Krishnil R.R., Sunil P.L., Rafiuddin Ahmeda M., "Design and optimization of airfoils and a 20 kW wind turbine using multiobjective genetic algorithm and HARP_Opt code," Renewable Energ, 2018.

[6] Xu Z., Zheng W., Wei L., Zituo W., Mateusz B., "Design optimization of a blunt trailing-edge airfoil," Alexandria Engineering Journal, vol. 65, pp. 887-896, 2023.

[7] Xingxing L., Lei Z., Juanjuan S., Fengjiao B., Ke Y., "Airfoil design for large horizontal axis wind turbines in low wind," Renewable Energy, vol. 145, pp. 2345-2357, 2019.

[8] Abdelaty, M.E., Osman A.M., Abdellatif, O.E., "Numerical Investigation of the Performance of Twisted and Untwisted Blades for Small Horizontal axis Wind Turbines," Faculty of Engineering at Shoubra, vol. 1, 2015.

[9] Mohamed, E.A.E.A, Abdellatif, O.E. and Osman, A.M, "Experimental and numerical investigation into effect of different blade configurations on performance of small-scale wind turbines," Energy Reports, vol. 7, pp. 138–143, 2021.

[10] Mohammed G.K., Aboelyazied M.K., "Effect of dust on the performance of wind turbines," Desalination, vol. 209, pp. 209–220, 2007.

[11] Hoksbergen, T.H., Akkerman, R., Baran, I., "Liquid droplet impact pressure on (elastic) solids for prediction of rain," Journal of Wind Engineering & Industrial Aerodynamics, vol. 233, pp. 105319, 2023.

[12] Linyue G., Yang L., Wenwu Z., Hui H., "An Experimental Study on the Aerodynamic Performance Degradation of a Wind Turbine Blade Model Induced by Ice Accretion Process," Renewable Energy, 2018.

[13] Abdulkareem O.A., Ahmed F.K. and Ali S.A., "Numerical Investigation of the Effect of Changing the Thickness," IOP Conf. Series: Materials Science and Engineering, vol. 1094, pp. 012078, 2021.

[14] Haseeb S., Nikesh B., Sathyajith M., Chee M.L., "Low Reynolds Number Airfoil for Small Horizontal Axis Wind Turbine Blades," Innovations for Sustainable and Secure Energy, pp. 21-23, 2012.

[15] Nhung, L.T. T., Van Y, N., Cong Truong, D., & Dinh Quy, V. (2024). CFD analysis of key factors impacting the aerodynamic performance of the S830 wind turbine airfoil. International Journal of Renewable Energy Development, 13(6), 1068-1077. https://doi.org/10.61435/ijred.2024.60249

[16] ANSYS Help. [Online]. Available: https://ansyshelp.ansys.com.